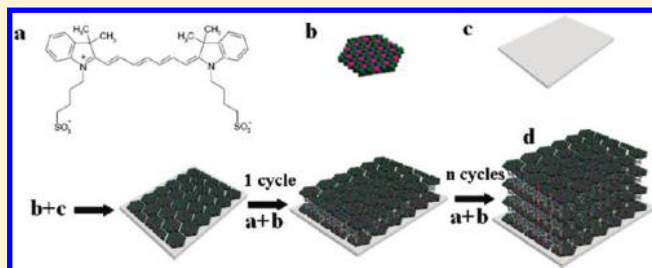


Near-Infrared Absorption and Polarized Luminescent Ultrathin Films Based on Sulfonated Cyanines and Layered Double Hydroxide

Dongpeng Yan,[†] Jun Lu,^{†,*} Jing Ma,[‡] Min Wei,^{†,*} Shuangde Li,[†] David G. Evans,[†] and Xue Duan[†][†]State Key Laboratory of Chemical Resource Engineering, Beijing University of Chemical Technology, Beijing, 100029, P. R. China[‡]School of Chemistry and Chemical Engineering, Institute of Theoretical and Computational Chemistry, Key Laboratory of Mesoscopic Chemistry of MOE, Nanjing University, Nanjing, 210093, P.R. China

Supporting Information

ABSTRACT: Organic–inorganic hybrid ultrathin films (UTFs) were fabricated by alternate assembly of sulfonated carbocyanine derivate (Scy) and exfoliated Mg–Al-layered double hydroxide (LDH) monolayers via layer-by-layer (LbL) method, which show uniform near-infrared (NIR) absorption and photoluminescence properties. UV–vis absorption and fluorescence spectroscopy indicate a stepwise and regular growth of the UTFs upon increasing deposition cycles. X-ray diffraction demonstrates that the UTFs possess periodical layered structure with the basal spacing of 3.3 nm; scanning electron microscopy and atomic force microscopy show that the UTFs surface are microscopically smooth and uniform. The Scy/LDH UTFs exhibit well-defined polarized photoemission character with the maximum luminescence anisotropy as high as ~0.8. Moreover, the Scy/LDH UTFs display higher stability than the pristine Scy, suggesting that the existence of LDH nanosheets enhance the thermal performance of the Scy dye. A molecular dynamics study was carried out to investigate the basal spacing and arrangement of Scy in the UTFs, and the results show that the Scy anions preferred to arrange within the LDH monolayer, which favor the improvement of the NIR polarized luminescence anisotropy of the Scy anions. Therefore, this work not only gives a facile method for fabricating NIR absorption and luminescence ultrathin film system but also provides a detailed understanding of the geometric structure of NIR photofunctional anions confined between the LDH monolayers.



1. INTRODUCTION

The organic materials with near-infrared (NIR) absorption and fluorescence properties have received growing attention during last few decades because of their great potential in both fundamental research and industrial applications.^{1–5} For instance, the NIR absorption materials can be used in the field of laser-welding of plastics or efficient blocking of heat rays.¹ The NIR fluorescent materials have also been the subject of recent interest in the range from biological optical imaging² to light-emitting diodes.³ Generally, these NIR materials mainly include the lanthanide metal complexes and low-band gap fluorescent dyes or polymers. Since the luminescent efficiency of the lanthanide metal complexes is not high enough owing to the parity-forbidden 4f–4f transitions, the organic fluorescent dyes have been widely used as NIR materials.⁴ However, the organic dyes generally display the following disadvantages: first, their absorption and luminescence performances are not satisfactory due to their insufficient thermal and chemical stability; second, the aggregation of dyes owing to the aromatic π – π interactions results in the fluorescence red-shift, broadening or even quenching; third, their low band gap leads to strong nonradiative relaxation (excitonic coupling and excimer formation), which is detrimental to their optical applications. To overcome or

compensate these disadvantages, great efforts have been devoted to design and synthesize new types of NIR derivatives;¹ unfortunately, the time-consuming synthesis process and relative low yield often restrict their application. Therefore, it is of crucial importance to achieve novel NIR materials with high thermal/chemical stability and enhanced optical properties.

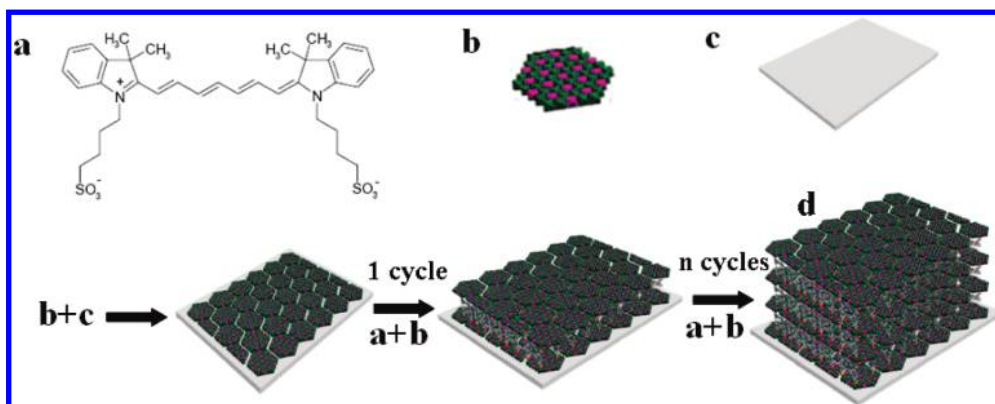
Recently, considerable interest has been focused on the fabrication of 2D ordered inorganic–chromophore thin film materials, for they may show novel functionalities (such as enhanced photo-, thermal-, and mechanical-stabilization) compared with their individual components alone.⁶ In this sense, layered double hydroxides (LDHs), whose structure can be generally expressed as the general formula $[M^{II}_{1-x}M^{III}_x(OH)_2]^{z+}A^{n-}_{z/n} \cdot \gamma H_2O$ (M^{II} and M^{III} are divalent and trivalent metals respectively, A^{n-} is the guest anion), are one type of important layered matrixes with a large versatility based on their tunable layered charge density and chemical composition.⁷ Moreover, the exfoliated LDH nanosheets also serve as the promising building blocks for constructing various 2D-organized functional nanocomposite.⁸

Received: January 7, 2011

Revised: March 23, 2011

Published: April 01, 2011

Scheme 1. a) Chemical Structure of Scy; b) the Representation of One Monolayer of Mg–Al-Layered Double Hydroxide (Mg–Al-LDH) (Dark Pink: Al(OH)₆ Octahedron; Green: Mg(OH)₆ Octahedron); c) the Substrate and d) the Resulting (Scy/LDH)_n UTF



Several visible luminescent molecules, such as organic anions,⁹ π -conjugated polymers¹⁰ and photoactive complexes,¹¹ have been assembled with LDH nanosheets to achieve luminescent materials with superior optical performances and improved luminous efficiency owing to the host–guest interactions. Furthermore, the preferential orientation of dye molecules between the LDH nanosheets can exhibit specific anisotropic photoemission characteristics, due to the intrinsic anisotropy of the LDHs with 2D lamellar structure.¹² To the best of our knowledge, however, the incorporation of NIR dye anions into LDH nanosheets to obtain polarized luminescence properties has scarcely been reported.

Carbocyanine (Cy) dyes and their derivatives, at present, are the most commonly used NIR materials. Their tunable spectral properties, large molar extinction coefficients, and high quantum yields make them good candidates as molecular probe and NIR fluorescent materials.⁵ Nevertheless, the aggregation of Cy dyes in the solid state usually leads to fluorescence quenching, which greatly restricts their application in solid-state NIR absorption and fluorescence devices. The LBL assembly principle enlightens and inspires us to challenge the goal of alternate deposition of Cy with LDH nanosheets to obtain one new type of NIR thin film materials, which would exhibit the following advantages: (1) the positively charged LDH monolayer provides NIR dye anions with an ordered microenvironment to isolate the anions between adjacent layers and may reduce the π – π stacking interaction;^{9b} (2) the presence of inorganic LDH monolayers can improve the thermal and optical stability of the interlayer NIR dye, which meet the requirement of long-term application; (3) the rigid and confined space imposed by LDH monolayers can suppress the thermal vibration and rotation of NIR anions relating to the non-radiative relaxation process of their exciting states.^{10b}

In this work, an ordered alternate assembly of a sulfonated derivate of Cy (Scy, 2-[7-(1,3-dihydro-3,3-dimethyl-1-(4-sulfobutyl)-2H-indol-2-ylidene)-1,3,5-heptatrienyl]-3,3-dimethyl-1-(4-sulfobutyl)-3H-indolium, inner monosodium salt, part a of Scheme 1) and exfoliated Mg–Al-LDH nanosheet (part b of Scheme 1) has been achieved to fabricate the (Scy/LDH)_n ($n = 4$ – 32) ultrathin films (UTFs, part d of Scheme 1) by the LBL method. The obtained (Scy/LDH)_n UTFs show well-defined NIR absorption and fluorescence properties. They exhibit long-range ordered structure and higher thermal/chemical stability than the pristine Scy samples; moreover, it was found that the NIR polarized photoluminescence can be obtained from

the UTFs. In addition, molecular dynamics (MD) simulation based on a modified cff91 forcefield¹³ was employed to analyze the basal spacing and orientation of the confined Scy anions within the LDH matrix. The simulation results illustrate that the Scy anions arranged uniformly and orderly between the LDH monolayers, which are in reasonable agreement with the experimental results, demonstrating the feasibility of MD simulation for this NIR dye/LDH system. Therefore, this work not only achieves the ordered assembly of UTFs with prospective NIR absorption and polarized luminescent applications based on the supramolecular architecture of Scy and LDH monolayers, but also provides a detailed understanding of the geometric structure and preferential arrangement of NIR species confined between the sheets of LDHs.

2. EXPERIMENTAL SECTION

2.1. Reagents and Materials. Sulfonated derivate of cyanine (Scy: 2-[7-(1,3-dihydro-3,3-dimethyl-1-(4-sulfobutyl)-2H-indol-2-ylidene)-1,3,5-heptatrienyl]-3,3-dimethyl-1-(4-sulfobutyl)-3H-indolium, inner monosodium salt) was purchased from American Dye Source, Inc. Analytical grade Mg (NO₃)₂·6H₂O, Al (NO₃)₃·9H₂O and urea were purchased from Beijing Chemical Co. Ltd. and used without further purification.

2.2. Fabrication of the (Scy/LDH)_n UTFs. The processes of synthesis and exfoliation of Mg–Al-LDH were similar to that described in our previous work.¹⁰ Mg–Al-LDH (0.1 g) was shaken in 100 cm³ of formamide solution for 24 h to produce a colloidal suspension of exfoliated Mg–Al-LDH nanosheets. The quartz glass substrate was cleaned in concentrated NH₃/30% H₂O₂ (7:3) and concentrated H₂SO₄ for 30 min each and washed thoroughly with deionized water. The substrate was dipped in a colloidal suspension (1 g dm⁻³) of LDH nanosheets for 10 min followed by washing thoroughly, and then was immersed into a 100 mL of Scy aqueous solution (0.1 g dm⁻³) for another 10 min. Multilayer films of (Scy/LDH)_n were fabricated by alternate deposition of LDH nanosheets and Scy anions for n cycles. The resulting films were dried under a nitrogen gas flow at 25 °C.

2.3. Sample Characterization. The UV–vis absorption spectra were collected in the range from 190 to 900 nm on a Shimadzu U-3000 spectrophotometer, with the slit width of 1.0 nm. The fluorescence spectra were performed on a RF-5301PC fluorospectrophotometer with the excitation wavelength of 740 nm.

The fluorescence emission spectra range in 765–840 nm, and both the excitation and emission slit are set to be 5 nm. Steady-state polarized photoluminescence measurements of the Scy/LDH UTFs were recorded with an Edinburgh Instruments' FLS 920 fluorospectrophotometer. The excitation and emission light keep 0° and 90° with respect to the thin film, respectively; that is, a glancing incidence geometry was employed to determine the luminescence anisotropy. X-ray diffraction patterns (XRD) of the Scy/LDH UTFs were recorded using a Rigaku 2500VB2+PC diffractometer under the conditions: 40 kV, 50 mA, Cu K α radiation ($\lambda = 0.154056$ nm) with step-scanned in step of 0.04° (2θ) in the range from 2 to 12° using a count time of 10 s/step. The morphology of thin films was investigated by using a scanning electron microscope (SEM Hitachi S-3500) equipped with an EDX attachment (EDX Oxford Instrument Isis 300), and the accelerating voltage applied was 20 kV. The surface roughness and thickness data were obtained by using the atomic force microscopy (AFM) software (Digital Instruments, Version 6.12). Thermogravimetry and differential thermal analysis (TG-DTA) measurement was performed on the Scy intercalated LDH sample prepared by the coprecipitation method.^{13a} A PCT-1A thermal analysis system under ambient atmosphere with a heating rate of $10^\circ\text{C}/\text{min}$ was employed.

2.4. Building of the Structural Model for the Scy/LDH System and Computational Method. An ideal LDH layer with $R3\text{-}m$ space group containing 48 Mg atoms and 24 Al atoms was built. The lattice parameters of the 2D layer are $a = b = 3.05$ Å, in accordance with other literatures.¹⁴ Each octahedral layer has 72 metal atoms and 144 OH groups, and a supercell was constructed with lattice parameter $a = 36.60$ Å, $b = 18.30$ Å, and the initial interlayer spacing $c = 32$ Å (experimental result), $\alpha = \beta = 90^\circ$, $\gamma = 120^\circ$ (equivalent to a $12 \times 6 \times 1$ supercell). The supercell was treated as $P1$ symmetry, and a 3D periodic boundary condition was applied.¹⁵ Then, 24 anionic Scy ($\text{C}_{35}\text{H}_{43}\text{N}_2\text{O}_6\text{S}_2$) with one negative charge each, were introduced into the simulated supercell, in which their sulfonatopropoxy groups are normal to the LDH layers. As a result, the formula of the simulated structure can be expressed as: $\text{Mg}_{48}\text{Al}_{24}(\text{OH})_{144}(\text{C}_{35}\text{H}_{43}\text{N}_2\text{O}_6\text{S}_2)_{24}$.

A modified cff91 forcefield¹³ was employed to perform MD simulation in the whole process. Charge equilibration (QEq) method¹⁶ was used to calculate atomic charges of the layer, in which the partial charges are $+0.703e$ for Mg, $+1.363e$ for Al, $-0.537e$ for O, and $+0.243e$ for H. Other forcefield parameters for the anions and water molecules were referred to the cff91 forcefield.¹⁷ The NBO analysis¹⁸ was employed to calculate the partial charges of Scy anion on B3LYP/6-31G** level using the Gaussian 03 programs.¹⁹ For water molecule, the partial charges came from the simple point charge (SPC) water model.²⁰ In potential energy calculations, the long-range coulomb interactions between partial charges were computed by the Ewald summation technique^{15a} and a spline cutoff method was used to calculate van der Waals interaction. After energy minimization was applied on the initial model, MD simulations were performed in isothermal–isobaric (NPT) ensemble with the temperature of 300 K and the pressure of 0.1 MPa (about 1 atm). The Andersen method²¹ and Berendsen method²² were used to control temperature and pressure, respectively. The total simulation time was 300 ps with the simulation time step of 1 fs. The result shows that the system reached equilibrium with lattice parameters and total potential energy fluctuating around a constant value within the first 50 ps, so the dynamic trajectories were recorded every 20 fs in the remaining 250 ps in order to analyze the ensemble average values. All the simulations were

performed using Discover module in *Material Studio* software package.²³ The LUMO (lowest unoccupied molecular orbital) and HOMO (highest occupied molecular orbital) energy levels of the Scy were performed with the density functional theory (DFT) method using Dmol3^{24a,b} module in *Material Studio* software package.^{24c} The initial configuration was fully optimized by Perdew–Wang (PW91)^{24d} generalized gradient approximation (GGA) method with the double numerical basis sets plus polarization function (DNP). SCF converged criterion was within 1.0×10^{-5} hartree/atom and converged criterion of structure optimization was 1.0×10^{-3} hartree/bohr.

3. RESULTS AND DISCUSSION

3.1. Assembly of the Scy/LDH UTFs. Part a of Figure 1 shows the UV–vis absorption spectra of the as-prepared $(\text{Scy}/\text{LDH})_n$ UTFs with various bilayer numbers (n) deposited on quartz substrates. It can be observed that the maximum characteristic absorption bands of Scy (~ 775 nm), is located within the NIR region, whose intensity correlates linearly with n (insert of part a of Figure 1). This indicates a stepwise and regular deposition procedure with almost equal amounts of Scy anions incorporated in each cycle. This was further confirmed by the gradual enhancement in color upon the increase of bilayers (insert of part a of Figure 1). The sharp NIR fluorescence peak of $(\text{Scy}/\text{LDH})_n$ UTF appears at ~ 785 nm and displays consistent increase along with n (part b of Figure 1). Compared with the Scy pristine solution (Figure S1 of the Supporting Information), no obvious red or blue shift of the fluorescence spectra was observed for the as-prepared UTFs with different bilayers, indicating the absence of Scy aggregates throughout the whole assembly process. This can be attributed to the isolation effect on the Scy anions imposed by the rigid LDH nanosheets, which eliminates the interlayer π – π stacking interaction. All of these results show that the as-prepared Scy/LDH UTF system exhibit NIR absorption and luminescent properties.

3.2. Structural and Morphology Characterization. X-ray diffraction reflection of the as-prepared UTFs appears at ca. 2.6° (part a of Figure 2), and the peak intensity increases upon increasing the bilayer number, indicating that the UTFs present an orderly periodical structure in the normal direction of the film with a period of 3.28 nm. This value is approximately consistent with the basal spacing of Scy intercalated LDH powder sample (d_{003} : ~ 3.0 nm) prepared by the coprecipitation method (Figure S2 of the Supporting Information). Moreover, this result is also in agreement with the ideal double-layered arrangement model of the Scy/LDH supermolecular structure with the thickness of ~ 0.48 nm for LDH monolayer and 1.19 nm for the extended chain configuration of Scy (part b of Figure 2). The double-layer arrangement mode of the Scy in the LDH gallery is related to its chemical structure. The Scy molecule possesses one polar end and one nonpolar end, respectively. The nonpolar group does not favor to assemble with positively charged LDH layer, resulting in the double-layer arrangement mode within the ultrathin film. Similar behavior was also observed in an anionic poly(p-phenylenevinylene)/LDH ultrathin film.^{10b} The deposition process of $(\text{Scy}/\text{LDH})_n$ UTFs was further monitored by scanning electron microscopy (SEM, Figure S3 of the Supporting Information) and atomic force microscopy (AFM). The thickness of the as-prepared UTFs ($n = 8$ – 32) are in the range 28–108 nm (Figure S4 and Table S1 of the Supporting

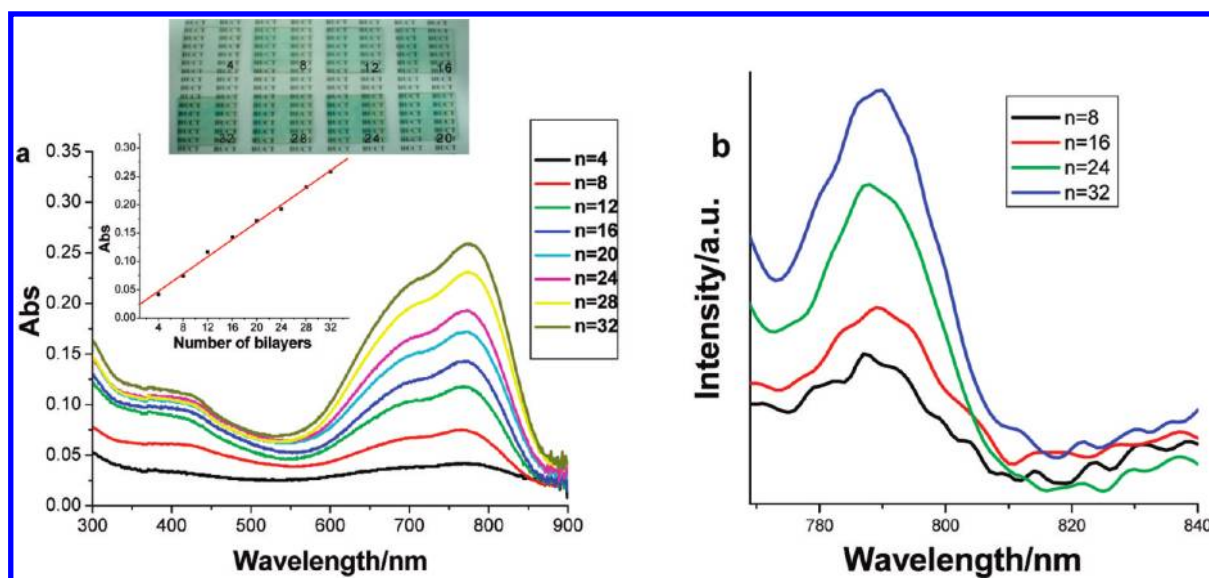


Figure 1. Characterization of the $(\text{Scy/LDH})_n$ ($n = 4\text{--}32$) UTFs: a) UV-vis absorption spectra (the insert shows the absorbance at 775 nm vs n and the photograph of UTFs with different bilayer number under daylight), b) fluorescence spectra.

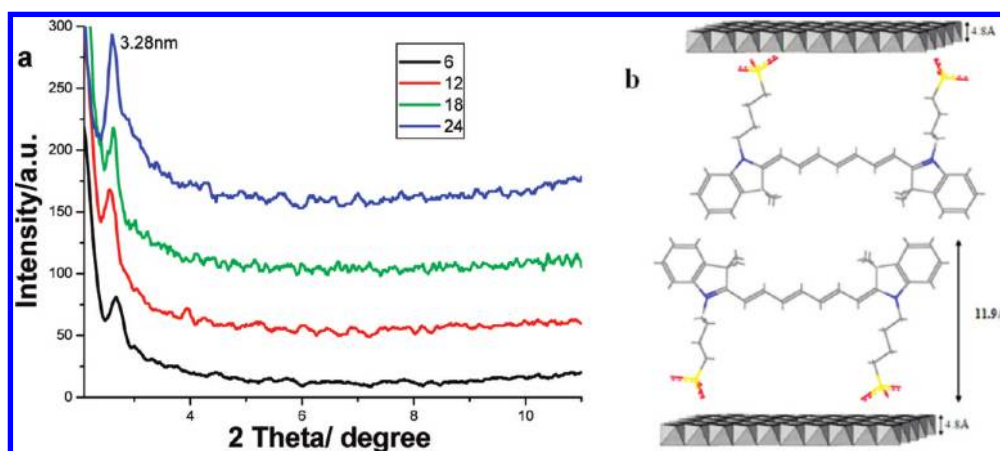


Figure 2. a) Small angle XRD patterns for the $(\text{Scy/LDH})_n$ UTFs with 8, 16, 24, 32 bilayers; b) the structural model of Scy/LDH.

Information). The approximately linear increase of the thickness upon increasing bilayer number confirms that the UTFs present uniform and periodic layered structure, in agreement with the behavior revealed by absorption and fluorescence spectra above. The typical top view of low-magnification (part a of Figure 3) and high-magnification (insert in part a of Figure 3) SEM image for the $(\text{Scy/LDH})_{32}$ UTF shows that the film surface is microscopically smooth and uniform; moreover, the continuous and homogeneous UTF can also be observed from its side view of SEM image (part b of Figure 3), with the thickness of 108 nm. It thus can be estimated that the thickness of one bilayer $(\text{Scy/LDH})_1$ is ca. 3.38 nm, which also agrees well with that of the XRD result. The AFM topographical and phase images shown in parts c and d of Figure 3 ($2 \times 2 \mu\text{m}^2$) give the morphology and roughness information of the UTF, from which a root-mean square roughness of 15.68 nm was obtained. Additionally, the surface roughness of the as-prepared UTFs ($n = 8\text{--}32$) ranges in 4.96–15.68 nm (Table S1 of the Supporting Information), suggesting that the surface roughness increases upon increasing the assembled bilayer.

Thermolysis behavior of the pristine Scy was studied as a reference to compare with Scy/LDH system, and its thermogravimetric and differential thermal analysis (TG-DTA) curves are displayed in part a of Figure 4. The sharp weight loss with two peaks at ~ 520 and 598 °C in the DTA curve is attributed to the decomposition and combustion of Scy. In the case of the Scy/Mg–Al-LDH sample (part b of Figure 4), a strong exothermic peak occurs at ~ 636 °C, indicating that the thermal stability of Scy molecule is enhanced greatly upon assembly with the LDH nanosheets.

3.3. Polarized Fluorescence of the UTFs. The orderly assembly and well-defined crystal structure of the Scy/LDH UTFs further inspired us to exploit their polarized luminescence properties. The glancing incidence geometry (insert in part b of Figure 5) were employed to determine the luminescence anisotropic value r .²⁵ For the sample of pristine Scy aqueous solution, the r value is ~ 0.2 in the range from 760 to 820 nm (Figure S5 of the Supporting Information), which is much higher than that of other luminescent dyes solution.¹² The uniform r value of ~ 0.2 for the dye in aqueous solution is related to the random

distribution of the dye molecules in the nonviscous liquid. Importantly, the (Scy/LDH)₈ UTF shows NIR polarized

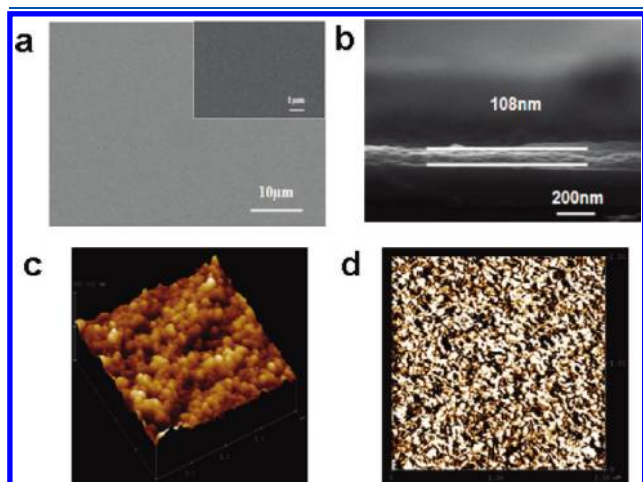


Figure 3. Morphology of (Scy/LDH)₃₂ UTF: (a) top view and (b) side view SEM image, (c) and (d) are the tapping-mode AFM topographic and phase image.

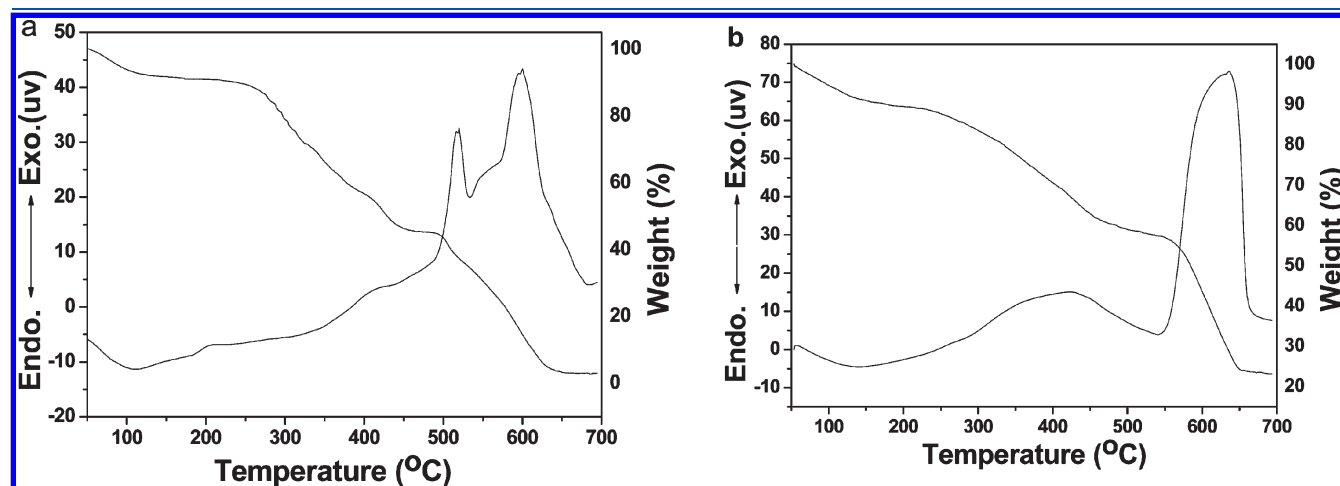


Figure 4. TG and DTA curves for a) pristine Scy, b) Scy/Mg–Al-LDH.

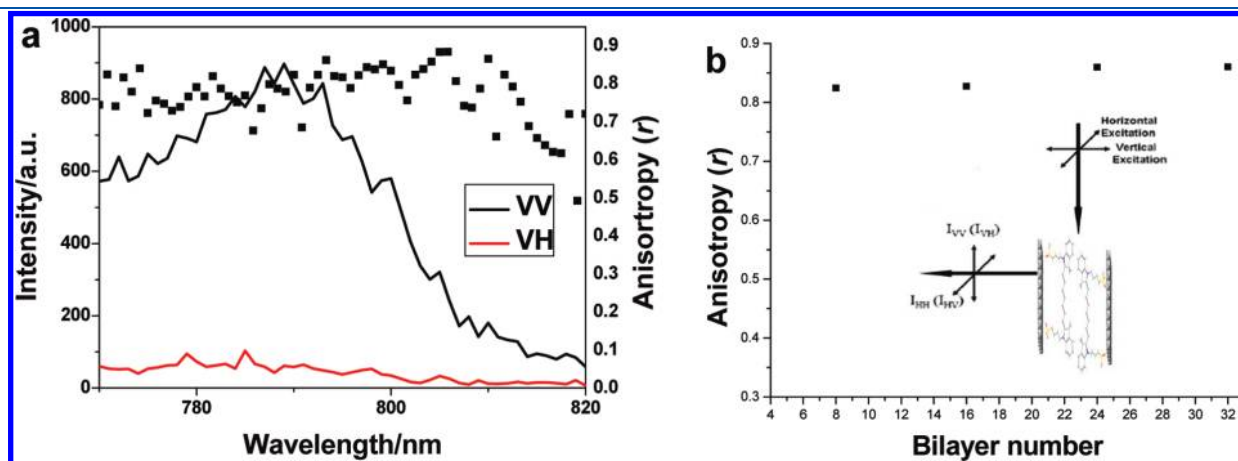


Figure 5. a) Polarized fluorescence profiles in the VV, VH modes and anisotropic value (r) for the (Scy/LDH)₈ UTF. b) The correlation between fluorescence anisotropic values (r) of the Scy/LDH UTFs (averaged in the range 770–810 nm) and the bilayer number in the measurement mode with glancing incidence geometry.

fluorescence (part a of Figure 5) between the parallel and perpendicular to excitation polarized direction (I_{VV} vs I_{VH}) with the anisotropic value (r) of ~ 0.8 (nearly twice than the theoretical highest value of 0.4 for the system without macroscopic alignment^{11,25b}), further demonstrating the ordered arrangement of Scy anions in the gallery of LDH monolayer. Furthermore, the r value is nearly independent of the bilayer number (part b of Figure 5b), indicating that the film thickness imposes no obvious influence on the macroscopic polarized luminescence of Scy/LDH UTFs throughout the whole assembly process.

3.4. Theoretical Study

3.4.1. Properties of Scy Anion. The optimal configuration of Scy shows that the length of its long axis is ~ 2.11 nm. The HOMO and LUMO profiles for Scy are shown in Figure 6. It can be observed that the frontier orbitals of Scy are mainly distributed on the main conjugated chain, illustrating that the transition moment involving the absorption and excitation/emission of Scy are located in its long axis direction. The calculated molecular orbital energies (relative to the vacuum energy level) are -5.13 (HOMO) and -3.69 eV (LUMO), respectively. The energy gap [$\Delta E_g = E(\text{LUMO}) - E(\text{HOMO})$] is ~ 1.44 eV, which is close to the maximum absorption of Scy/LDH at 775 nm (1.60 eV).

3.4.2. Basal Spacing and Arrangement of Scy in the Gallery of LDH. The basal spacing of the Scy/LDH UTFs was calculated for further comparison with the experimental results. The simulated basal spacing is ~ 3.42 nm, which is very close to that of the experimental value (3.28 nm), confirming the feasibility of MD simulation for the Scy/LDH system. The orientation of Scy anions in the LDH galleries is an important parameter for understanding the order degree of Scy anions in a confined environment. Angle θ_1 stands for the orientational angle of the lineation between the N atoms in Scy with respect to the LDH

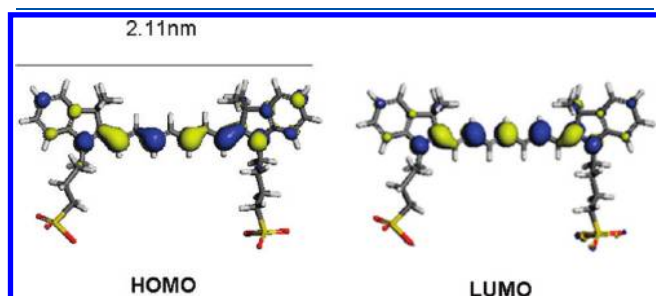


Figure 6. HOMO and LUMO profiles for Scy.

monolayer (insert in part a of Figure 7), which varies between 3.9° and 13.8° with the most probable angle of $\sim 10.2^\circ$. This is consistent well with the value (8.3°) determined by the polarized fluorescence method (Figure S6 of the Supporting Information). This suggests that the long-axis of the Scy anions is nearly parallel to the LDH monolayer, accounting for the high emission anisotropy of the Scy/LDH UTF revealed in the experimental observation. The θ_2 was defined as the angle of C_1C_2S in the side-chain of Scy anions as shown in the insert of part b of Figure 7. Compared with the pristine Scy anion ($\sim 142.8^\circ$) calculated by the DFT method, the maximum value of θ_2 appears at 155.0° . The obvious change in θ_2 indicates that the strong electronic interaction allow the negatively charged sulfonate groups to anchor to the positively charged LDH monolayers.

To further understand the atom distribution of interlayer molecules and the polar/nonpolar character, the distribution of N and S along the direction normal to the LDH monolayer was calculated. The typical density profile is shown in part a of Figure 8. It was observed that the N and S profiles display nearly symmetric distribution in the gallery of LDH. The distribution of S atom in the sulfonate group is consistent with the electrostatic interaction mode between the sulfonate group and the positive-charged LDH host layer, which supply a polar environment.

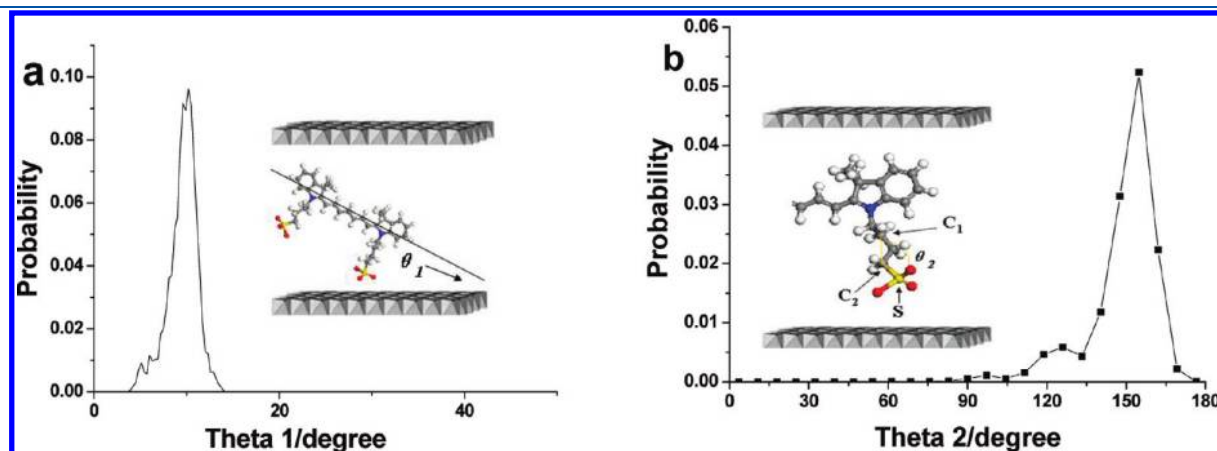


Figure 7. a) Distribution of the orientation angle θ_1 (the N–N lineation in the Scy with respect to the LDH layer), b) the distribution of the orientation angle θ_2 (C_1C_2S in side-chain of the Scy anion).

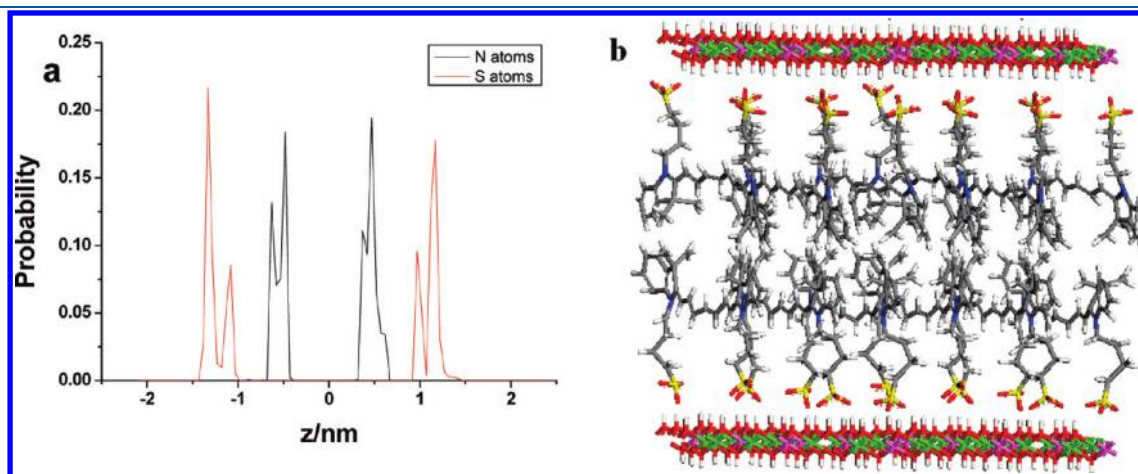


Figure 8. a) Distribution probability of N and S atoms in the Scy within the LDH layers in the z direction. The center of the interlayer gallery is chosen as the origin of coordinates, b) a snapshot of the Scy/LDH system.

The typical snapshot of the configuration for the Scy/LDH system is shown in part b of Figure 8, from which it can be observed that all the Scy anions aligned regularly and orderly within the monolayers.

4. CONCLUSIONS

In summary, the ordered (Scy/LDH)_n UTFs were fabricated, which show well-defined NIR absorption and photoluminescence properties. The XRD, SEM, and AFM confirm that the Scy anions exhibit regular and ordered alignment within the LDH nanosheets; therefore the NIR polarized luminescence with the anisotropy as high as 0.8 was obtained for the UTFs. In addition, TG-DTA shows that the thermal stability of Scy anions is enhanced upon assembly with the LDH nanosheets. DFT calculation reveals that the Scy anion has low band gap, and the frontier orbitals are mainly populated in the main conjugated chain of Scy. Molecular dynamics simulation demonstrates that the confined Scy anions are nearly parallel with respect to the LDH monolayer, which endows the high NIR anisotropy of the Scy anions. Therefore, this work provides a facile way to design and fabricate novel organic–inorganic UTF architectures with NIR absorption and polarized photoluminescence properties, which can be potentially used in various opto-electrical devices.

■ ASSOCIATED CONTENT

S Supporting Information. Figures of emission spectrum of Scy aqueous solution, powder XRD pattern of the Scy/Mg–Al-LDH composite prepared with the coprecipitation method, top view of low-magnification and high-magnification SEM images for the Scy/LDH UTFs, side view of SEM image for the Scy/LDH UTFs; polarized fluorescence profiles in the VV, VH modes and anisotropic value (*r*) for the Scy aqueous solution; table of depth and thickness parameters for the UTFs; figure of evolution of the fluorescence dichroic ratio of the as-prepared (Scy/LDH)₃₂ film with the emission wavelength for different twist angles δ of the sample. This material is available free of charge via the Internet at <http://pubs.acs.org>.

■ AUTHOR INFORMATION

Corresponding Author

*E-mail: lujun@mail.buct.edu.cn (J.L.); e-mail: weimin@mail.buct.edu.cn (M.W.), fax: +86-10-64425385, tel: +86-10-64412131.

■ ACKNOWLEDGMENT

This work was supported by the National Natural Science Foundation of China, the 111 Project (Grant No.: B07004), and the 973 Program (Grant No.: 2011CBA00504).

■ REFERENCES

- (1) Pschirer, N. G.; Kohl, C.; Nolde, F.; Qu, J.; Müllen, K. *Angew. Chem., Int. Ed.* **2006**, *45*, 1401.
- (2) Tessler, N.; Medvedev, V.; Kazes, M.; Kan, S.; Banin, U. *Science* **2002**, *295*, 1506.
- (3) Johnson, J. R.; Fu, N.; Arunkumar, E.; Leevy, W. M.; Gammon, S. T.; Worms, D. P.; Smith, B. D. *Angew. Chem., Int. Ed.* **2007**, *46*, 5528.
- (4) Qian, G.; Dai, B.; Luo, M.; Yu, D.; Zhan, J.; Zhang, Z.; Ma, D.; Wang, Z. *Chem. Mater.* **2008**, *20*, 6208.
- (5) Zhang, Z.; Berezin, M. Y.; Kao, J. L. F.; Avignon, A. d'; Bai, M.; Achilefu, S. *Angew. Chem., Int. Ed.* **2008**, *47*, 3584.

- (6) Ogawa, M.; Kuroda, K. *Chem. Rev.* **1995**, *95*, 399.
- (7) (a) Fogg, A. M.; Green, V. M.; Harvey, H. G.; O'Hare, D. *Adv. Mater.* **1999**, *11*, 1466. (b) Evans, D. G.; Duan, X. *Chem. Commun.* **2006**, 485. (c) Gunawan, P.; Xu, R. *Chem. Mater.* **2009**, *21*, 781. (d) Lee, J. H.; Chang, J.; Cha, J. -H.; Jung, D. -Y.; Kim, S. S.; Kim, J. M. *Chem.—Eur. J.* **2010**, *16*, 8296. (e) Wang, J.; Song, Y.; Li, Z.; Liu, Q.; Zhou, J.; Jing, X.; Zhang, M.; Jiang, Z. *Energy Fuels* DOI:10.1021/ef101150b.
- (8) (a) Li, L.; Ma, R. Z.; Ebina, Y.; Iyi, N.; Sasaki, T. *Chem. Mater.* **2005**, *17*, 4386. (b) Liu, Z. P.; Ma, R. Z.; Osada, M.; Iyi, N.; Ebina, Y.; Takada, K.; Sasaki, T. *J. Am. Chem. Soc.* **2006**, *128*, 4872. (c) Huang, S.; Cen, X.; Peng, H.; Guo, S.; Wang, W.; Liu, T. *J. Phys. Chem. B* **2009**, *113*, 15225. (d) Chen, D.; Wang, X.; Liu, T.; Wang, X.; Li, J. *ACS Appl. Mater. Interfaces* **2010**, *2*, 2005. (e) Chen, D.; Huang, S.; Zhang, C.; Wang, W.; Liu, T. *Thin Solid Films* **2010**, *23*, 7081. (f) Zhu, H.; Huang, S.; Yang, Z.; Liu, T. *J. Mater. Chem.* **2011**, *21*, 2950. (g) Yan, D. P.; Lu, J.; Ma, J.; Wei, M.; Evans, D. G.; Duan, X. *Angew. Chem., Int. Ed.* **2011**, *50*, 720.
- (9) (a) Gago, S.; Costa, T.; de Melo, J. S.; Gonçalves, I. S.; Pillinger, M. J. *Mater. Chem.* **2008**, *18*, 894. (b) Yan, D. P.; Lu, J.; Ma, J.; Wei, M.; Qin, S.; Chen, L.; Evans, D. G.; Duan, X. *J. Mater. Chem.* **2010**, *20*, S016. (c) Wang, J.; Zhou, J.; Li, Z.; Liu, Q.; Yang, P.; Jing, X.; Zhang, M. *Mater. Res. Bull.* **2010**, *45*, 640.
- (10) (a) Yan, D. P.; Lu, J.; Wei, M.; Han, J. B.; Ma, J.; Li, F.; Evans, D. G.; Duan, X. *Angew. Chem., Int. Ed.* **2009**, *48*, 3073. (b) Yan, D. P.; Lu, J.; Ma, J.; Wei, M.; Evans, D. G.; Duan, X. *Langmuir* **2010**, *26*, 7007.
- (11) Yan, D. P.; Lu, J.; Wei, M.; Ma, J.; Evans, D. G.; Duan, X. *Chem. Commun.* **2009**, 6358.
- (12) (a) López Arbeloa, F.; Martínez, V.; Arbeloa, T.; López Arbeloa, I. *Reviews in Fluorescence* 2010, Chapter 1, 1–35; (b) Martínez Martínez, V.; Salleres, S.; Bañuelos, J.; López Arbeloa, F. *J. Fluoresc.* **2006**, *17*, 233. (c) Salleres, S.; López Arbeloa, F.; Martínez, V.; Arbeloa, T.; López Arbeloa, I. *J. Phys. Chem. C* **2009**, *113*, 965. (d) López Arbeloa, F.; Martínez Martínez, V. *J. Photochem. Photobiol., A* **2006**, *181*, 44. (e) López Arbeloa, F.; Martínez Martínez, V.; Arbeloa, T.; López Arbeloa, I. *J. Photochem. Photobiol., C* **2007**, *8*, 85. (f) Yan, D. P.; Lu, J.; Wei, M.; Evans, D. G.; Duan, X. *J. Phys. Chem. B* **2009**, *113*, 1381.
- (13) (a) Yan, D. P.; Lu, J.; Wei, M.; Li, H.; Ma, J.; Li, F.; Evans, D. G.; Duan, X. *J. Phys. Chem. A* **2008**, *112*, 7671. (b) Yan, D. P.; Lu, J.; Wei, M.; Ma, J.; Evans, D. G.; Duan, X. *Phys. Chem. Chem. Phys.* **2009**, *11*, 9200.
- (14) (a) Mohanambe, L.; Vasudevan, S. *J. Phys. Chem. B* **2005**, *109*, 15651. (b) Newman, S. P.; Williams, S. J.; Coveney, P. V.; Jones, W. *J. Phys. Chem. B* **1998**, *102*, 6710. (c) Káfuňková, E.; Taviot-Guêho, C.; Bezdučka, P.; Klementová, M.; Kovár, P.; Kubát, P.; Mosinger, J.; Pospíšil, M.; Lang, K. *Chem. Mater.* **2010**, *22*, 2481. (d) Yan, H.; Wei, M.; Ma, J.; Evans, D. G.; Duan, X. *J. Phys. Chem. A* **2010**, *114*, 7369.
- (15) (a) Allen, M. P.; Tildesley, D. J. *Computer Simulation of Liquids*; Clarendon: Oxford, 1987; (b) Leach, A. R. *Molecular Modeling, Principles and Applications*, 2nd ed.; Pearson Education Ltd: England, 2001. (c) Choi, S.; Coronas, J.; Jordan, E.; Oh, W.; Nair, S.; Onorato, F.; Shantz, D. F.; Tsapatsis, M. *Angew. Chem., Int. Ed.* **2008**, *47*, 552.
- (16) Rappé, A. K.; Goddard, W. A. *J. Phys. Chem.* **1991**, *95*, 3358.
- (17) Maple, J. R.; Hwang, M.-J.; Stockfisch, T. P.; Dinur, U.; Waldman, M.; Ewig, C. S.; Hagler, A. T. *J. Comput. Chem.* **1994**, *15*, 162.
- (18) Reed, A. E.; Curtiss, L. A.; Weinhold, F. *Chem. Rev.* **1988**, *88*, 899.
- (19) Frisch, M. J.; Trucks, G. W.; Schlegel, H. B.; Scuseria, G. E.; Robb, M. A.; Cheeseman, J. R.; Montgomery, J. A., Jr.; Vreven, T.; Kudin, K. N.; Burant, J. C.; Millam, J. M.; Iyengar, S. S.; Tomasi, J.; Barone, V.; Mennucci, B.; Cossi, M.; Scalmani, G.; Rega, N.; Petersson, G. A.; Nakatsuji, H.; Hada, M.; Ehara, M.; Toyota, K.; Fukuda, R.; Hasegawa, J.; Ishida, M.; Nakajima, T.; Honda, Y.; Kitao, O.; Nakai, H.; Klene, M.; Li, X.; Knox, J. E.; Hratchian, H. P.; Cross, J. B.; Adamo, C.; Jaramillo, J.; Gomperts, R.; Stratmann, R. E.; Yazyev, O.; Austin, A. J.; Cammi, R.; Pomelli, C.; Ochterski, J. W.; Ayala, P. Y.; Morokuma, K.; Voth, G. A.; Salvador, P.; Dannenberg, J. J.; Zakrzewski, V. G.; Dapprich, S.; Daniels, A. D.; Strain, M. C.; Farkas, O.; Malick, D. K.; Rabuck, A. D.; Raghavachari, K.; Foresman, J. B.; Ortiz, J. V.; Cui, Q.; Baboul, A. G.; Clifford, S.; Cioslowski, J.; Stefanov, B. B.; Liu, G.; Liashenko, A.

Piskorz, P.; Komaromi, I.; Martin, R. L.; Fox, D. J.; Keith, T.; Al-Laham, M. A.; Peng, C. Y.; Nanayakkara, A.; Challacombe, M.; Gill, P. M. W.; Johnson, B.; Chen, W.; Wong, M. W.; Gonzalez, C.; Pople, J. A. *Gaussian 03*, Revision B.04; Gaussian, Inc.: Pittsburgh, PA, 2003.

(20) Berendsen, H. J. C.; Postma, J. P. M.; van Gunsteren, W. F.; Hermans, J. Interaction models for water in relation to protein hydration. In *Intermolecular Forces*; Pullman, B., Ed.; Riedel: Dordrecht, The Netherlands, 1981; p 331.

(21) Andersen, H. C. *J. Chem. Phys.* **1980**, *72*, 2384.

(22) Berendsen, H. J. C.; Postma, J. P. M.; van Gunsteren, A.; Dinola, A.; Haak, J. R. *J. Chem. Phys.* **1984**, *81*, 3684.

(23) *Discover Module, MS Modeling*, Version 2.2; Accelrys Inc.: San Diego, CA, 2003.

(24) (a) Delley, B. *J. Chem. Phys.* **1990**, *92*, 508. (b) Delley, B. *J. Chem. Phys.* **2000**, *113*, 7756. (c) *Dmol3Module, MS Modeling*, Version 2.2; Accelrys Inc.: San Diego, CA, 2003; (d) Perdew, J. P.; Chevary, J. A.; Vosko, S. H.; Jackson, K. A.; Pederson, M. R.; Singh, D. J.; Fiolhais, C. *Phys. Rev. B* **1992**, *46*, 6671.

(25) (a) $r = (I_{VV} - GI_{VH}) / (I_{VV} + 2GI_{VH})$, where $G = I_{HV} / I_{HH}$, determined from the Scy aqueous solution. I_{VH} stand for the photoluminescence intensity obtained with vertical excitation polarized and horizontal detection polarization, and I_{VV} , I_{HV} , I_{HH} are defined in a similar way. (b) Valeur, B. *Molecular Fluorescence: Principles and Applications*; Wiley-VCH: Verlag, 2001.